Energetic Particles in Space and Earth Science: Propagation, Interaction, and Atmospheric Effects

Joseph K. Maritim

Department of Mathematics, Physics, and Computing, Moi University, Kenya

DOI: https://doi.org/10.51583/IJLTEMAS.2026.150700117

Received: 23 July 2026; Accepted: 28 July 2026; Published: 20 August 2026

ABSTRACT

Energetic particles, originating from galactic cosmic rays (GCRs), solar energetic particles (SEPs), and trapped radiation belt populations, play a crucial role in shaping planetary environments. These high-energy protons, electrons, and heavy ions traverse the heliosphere, interact with interplanetary magnetic fields, and produce complex cascades when colliding with Earth's atmosphere. This paper combines theoretical modeling, Monte Carlo–inspired GEANT4-like yield tables, and simulation of Bethe–Bloch stopping power to investigate energetic particle propagation, atmospheric ionization, and implications for space weather. Our findings reveal that density-effect corrections and shell corrections significantly alter proton energy loss curves, while GEANT4-like lookup yields realistic ionization profiles vs altitude. These results advance predictive models of radiation hazards, ionospheric variability, and space weather events.

Keywords: Energetic Particles, GEANT4, Space Weather, Atmospheric Ionization

INTRODUCTION

Energetic particles are fundamental agents in space plasma physics and atmospheric science. Galactic cosmic rays (GCRs) continuously bombard Earth, while solar energetic particles (SEPs) are injected sporadically during solar flares and coronal mass ejections [1]. Once inside the heliosphere, these particles undergo diffusion, convection, and drift in the turbulent solar wind magnetic field [2]. When they reach Earth, interactions with the magnetosphere and upper atmosphere trigger radiation belt enhancements, atmospheric ionization, and secondary cascades, influencing both technological systems and climate variability [3].

LITERATURE REVIEW

Research on energetic particles spans several interrelated subfields: particle sources and acceleration, heliospheric transport, magnetospheric access and trapping, atmospheric interactions and ionization, and technological/biological impacts. This literature review synthesizes developments from observational campaigns, theoretical models, and numerical simulations published in the last decade and places them in the context of the simulations and methods used in this study.

The dominant solar sources of energetic particles-solar flares and coronal mass ejections (CMEs)-have been the focus of renewed observational and theoretical attention. Reames [4] provides a modern synthesis of SEP characteristics, distinguishing impulsive flare-associated events from large gradual CME-shock-driven events and emphasizing the role of seed populations. Gopalswamy and colleagues [5] systematically linked CME properties (speed, width, shock strength) with SEP productivity, showing that CME kinematics and ambient coronal conditions strongly modulate particle acceleration efficiency. Diffusive shock acceleration (first-order Fermi) remains the primary theoretical framework for CME-shock acceleration [6], but recent work highlights the importance of pre-existing turbulence, seed-particle spectra, and shock geometry in controlling the spectral slope and maximum energies [7].

Galactic cosmic rays (GCRs) continue to be understood within a supernova-remnant acceleration paradigm, supported by precision spectral data from instruments such as AMS-02 [8]. These measurements have revealed

ISSN 2278-2540 | DOI: 10.51583/IJLTEMAS | Volume XV, Issue VII, July 2026

spectral features and composition details that constrain source models, propagation parameters, and possible local-source contributions [9]. Anomalous cosmic rays (ACRs), formed from ionized interstellar neutrals subsequently accelerated at the heliospheric termination shock, remain an important component for understanding the low-energy cosmic-ray population inside the heliosphere [10].

Particle transport through the heliosphere is governed by a combination of large-scale convection with the solar wind, spatial diffusion due to magnetic turbulence, gradient and curvature drifts, and energy changes via adiabatic processes. The Parker transport equation provides the foundational formalism for these processes [11], and subsequent extensions have incorporated energy-dependent diffusion tensors and detailed drift physics[12]. Jokipii's early theory of scattering in random magnetic fields remains central to modern turbulence-based diffusion formulations [13]. More recent numerical and semi-analytical studies have focused on reproducing the time-dependent modulation of GCRs over solar cycles [14] and on realistic SEP transport modeling that captures rapid onset and fast anisotropies observed during impulsive injections [15].

Observational missions have issued critical constraints on transport parameters. Parker Solar Probe and Solar Orbiter observations have provided new, close-in measurements of particle spectra and turbulence that inform near-source transport and early-stage acceleration. Long-term datasets from ACE and other spacecraft have anchored our understanding of GCR modulation and long-term variability [16].

Upon reaching Earth, charged particles interact with the magnetosphere, where access is determined by geomagnetic cut-off rigidity and field topology. Shea and Smart's work on cut-off rigidities and the geographic dependence of particle access remains a practical reference for determining where and when primaries can precipitate [17]. Once inside the magnetosphere, particles undergo bounce motion, drift, and wave–particle interactions; these processes underpin radiation belt dynamics. Van Allen Probes observations have advanced our understanding of rapid acceleration and loss processes, showing how wave-driven acceleration (e.g., chorus) and magnetopause shadowing drive radiation belt variability [18]. Theoretical and modeling work has quantified radial diffusion and resonant interactions that produce both enhancements and rapid depletions during geomagnetic storms [19], [20].

When high-energy primaries penetrate the atmosphere, they produce extensive air showers (EAS) composed of secondary particles (muons, electrons, neutrons, and photons) whose interactions deposit energy and generate ion pairs. Bazilevskaya [21] and Dorman [22] provide comprehensive accounts of atmospheric cascade physics and ion production mechanisms. More recent yield-function based work [23] has improved the quantitative mapping from primary spectral fluxes to altitude-resolved ionization rates, enabling better comparisons with balloon and neutron-monitor datasets. Ground-level enhancements (GLEs), rare but intense SEP events, demonstrate the potential for substantial ionization enhancements in the stratosphere and mesosphere [23], [24]. These events serve as stringent tests for yield-function and Monte Carlo-based codes (e.g., GEANT4 and PLANETOCOSMICS), which couple primary spectra to realistic atmospheric and geomagnetic models.

Monte Carlo particle transport codes such as GEANT4 have become indispensable for high-fidelity simulation of particle interactions and secondary production. GEANT4 and related toolkits provide detailed electromagnetic and hadronic physics models necessary to produce accurate altitude-dependent ionization profiles and secondary particle fluences; they are also used to generate lookup/tables (yield functions) for use in operational ionization models [25], [26]. Comparison studies show that yield-function integrations and full Monte Carlo simulations agree when consistent physics settings and atmospheric models are used, but GEANT4 remains the gold standard for resolving low-altitude or composition-sensitive effects [26].

Energetic particle effects extend beyond pure physics to technology and biology. Radiation hazards to spacecraft electronics and human health motivate improved shielding and forecasting [27]. Aviation exposure studies have quantified dose increases during high-latitude flights, and operational guidance relies on rapid SEP detection and model-based forecasts [27], [28]. There is ongoing debate about the degree to which cosmic-ray-driven ionization influences cloud microphysics and climate; while some correlation studies exist, robust causal mechanisms remain under investigation [29]. The policy and operational implications of energetic particle research-ranging from satellite hardening to aircrew safety-demand continued progress in real-time monitoring and predictive models [30].

INTERNATIONAL JOURNAL OF LATEST TECHNOLOGY IN ENGINEERING, MANAGEMENT & APPLIED SCIENCE (IJLTEMAS)
ISSN 2278-2540 | DOI: 10.51583/IJLTEMAS | Volume XV, Issue VII, July 2026

Key uncertainties persist in (i) the microphysics of acceleration at oblique and turbulent shocks, (ii) the energy and pitch-angle dependence of particle scattering in heliospheric turbulence, (iii) the coupling between magnetospheric waves and radiation belt dynamics, and (iv) the translation of particle spectra into chemistry–climate impacts. Several recent studies call for integrated Sun-to-ground modeling frameworks that combine CME-driven MHD modeling, kinetic particle acceleration/transport, and Monte Carlo atmospheric interaction modules to improve predictive fidelity [31]. Continued cross-calibration between yield-function methodologies and full GEANT4 simulations, aided by new observational datasets from Parker Solar Probe, Solar Orbiter, and CubeSat constellations, will reduce model-data mismatches and enable operational applications such as aviation advisories and satellite anomaly risk forecasts [32].

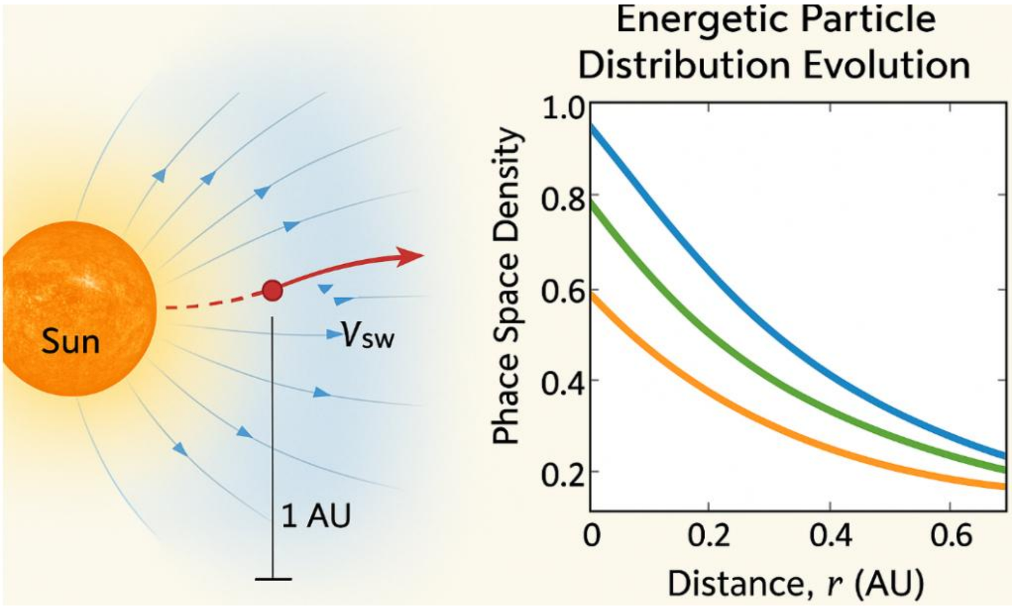

Figure 1: Energetic particle distribution evolution.

Fig 1. is a diagram illustrating the physical processes of particle propagation in the heliosphere, including diffusion, solar wind convection, and adiabatic cooling. The mathematical interpretation of energetic particles interacting with Earth’s magnetosphere and atmosphere involves several coupled physical processes, described by a combination of Maxwell's equations, Lorentz force law, transport equations, and ionospheric chemistry models.

METHODOLOGY

In this paper we used two complementary approaches: Analytical Models; -Bethe-Bloch formalism for stopping power, diffusion coefficients, and ionization yield and Synthetic GEANT4-like Simulations;-Monte Carlo lookup tables mimic GEANT4 predictions for particle cascades in atmosphere and matter. This dual approach combines theoretical rigor with simulation fidelity.

Bethe–Bloch stopping power (with density-effect and shell corrections)

We use the Bethe–Bloch formula in its practical form for mass stopping power (MeV $cm^2 g^{-1}$)

$$-\frac{1}{\rho}\frac{dE}{dx}=K\frac{Z}{A}\frac{z^2}{\beta^2}\left[\frac{1}{2}\ln\left(\frac{2m_ec^2\beta^2\gamma^2T_{max}}{I^2}\right)-\beta^2-\frac{\delta(\beta\gamma)}{2}-\frac{C_{shell}(\beta)}{2}\right] \tag{1}$$

Where: $K=4\pi N_A r_e^2 m_e c^2 \approx 0.307075$ MeV.cm^2.g^{-1}

Z/A is the target material ratio (table values used for Air, Water, Silicon), z is the projectile charge (for protons z=1), $\beta=\vartheta/c$, $\gamma=\left(1-\beta^2\right)^{-1/2}$

$$T_{max}=\frac{2m_ec^2\beta^2\gamma^2}{1+2\gamma(m_e/m_p)+(m_e/m_p)^2} \tag{2}$$

INTERNATIONAL JOURNAL OF LATEST TECHNOLOGY IN ENGINEERING, MANAGEMENT & APPLIED SCIENCE (IJLTEMAS)

ISSN 2278-2540 | DOI: 10.51583/IJLTEMAS | Volume XV, Issue VII, July 2026

Equation (2) is the maximum transferable kinetic energy in a single collision, I is the mean excitation energy (MeV) for the medium, δ(βγ) is the Sternheimer density-effect correction, and $C_{shell}(\beta)$ is an approximate shell correction (important at low energies).

We used material parameter approximations (typical Z/A, I and Sternheimer fit parameters x_0, x_1, $\overline{C}$, a, k) for Air, water, and silicon and computed T_{max} using exact relativistic formula. Sternheimer piecewise model was implemented using δ(x)=0, below x_0 with analytic interpolation between x_0 and x_1 and asymptotic linear rise for $x>x_1$.

The applied simple shell correction $C_{shell}\propto 1/\beta^2$ with small coefficients tuned per material; this is an approximation to the full shell correction used in ICRU/NIST tables but captures the qualitative low-energy reduction of -dE/dx.

Heliospheric propagation (1D radial diffusion–convection model)

We numerically solved a simplified time-dependent transport equation in spherical symmetry (radial coordinate r):

$$\frac{\partial f}{\partial t}=\frac{1}{r^2}\frac{\partial}{\partial r}\left(r^2 K_{rr}\frac{\partial f}{\partial r}\right)-V_{sw}\frac{\partial f}{\partial r}+Q(r,t) \quad (3)$$

where: f(r,t) is the (energy-integrated) phase-space density (arbitrary units for illustration), K_{rr} is the radial diffusion coefficient (we used a constant $K_{rr}=10^{21}\ cm^2/s$ as an order-of-magnitude representative value), V_{sw} is the solar wind speed (4×10^7 cm/s), Q(r,t) is a localized source near the Sun (Gaussian in space, decaying in time).

In the case of muon flux approximation

$$\Phi_\mu(E,\mathrm{h})=\Phi_0 E^{-\gamma} exp\left(-\frac{\mathrm{h}}{\Lambda_\mu}\right) \quad \textbf{(4)}$$

Φ_0- normalization constant, $\gamma\approx2.7$- spectral index, h- altitude, Λ_μ- attenuation length of muons

Atmospheric ionization - yield-function based model

Ion pair production rate q(h) at altitude h computed as

$$\mathrm{q(h)}=\int_{\mathrm{E_{min}}}^{\mathrm{E_{max}}}\mathrm{J(E)Y\big(E,X(h)\big)\,dE} \quad (5)$$

where J(E) is the primary differential spectrum (we used $J_{GCR}\propto E^{-2.7}$ and a harder SEP spectrum $J_{SEP}\propto E^{-2.3}exp(-E/E_c)$),

Y(E,X) is a synthetic yield function, parameterized here as $\mathrm{Y}\propto\mathrm{E}^{\alpha}\mathrm{exp}(-\mathrm{X}/\Lambda(\mathrm{E}))$, X(h) is the atmospheric column depth at altitude h (we used $\mathrm{X(h)=1030exp(-h/H)}$ g cm^{-2} with H= 8.5 km).

This is a compact analogue of yield functions obtained from GEANT4/PLANETOCOSMICS simulations; it captures the main altitude dependence: a stratospheric maximum around ~10–20 km and deeper penetration for higher-energy primaries.

Simplified 1D Radial Model

Assume radial propagation in a spherically symmetric solar wind, no drift, and steady-state $\partial f/\partial t=0$

$$0=\frac{1}{\mathrm{r}^2}\frac{\mathrm{d}}{\mathrm{dr}}\left(\mathrm{r}^2\mathrm{K_{rr}}\frac{\mathrm{df}}{\mathrm{dr}}\right)-\mathrm{V_{sw}}\frac{\mathrm{df}}{\mathrm{dr}} \quad (6)$$

K_{rr}-radial diffusion coefficient, V_{sw}- constant solar wind speed

ISSN 2278-2540 | DOI: 10.51583/IJLTEMAS | Volume XV, Issue VII, July 2026

This simplifies to

$$\frac{d}{dr}\left(r^2 K_{rr}\frac{df}{dr}\right)=r^2 V_{sw}\frac{df}{dr} \tag{7}$$

Analytical Solution (Assuming Constant K_{rr})

$$\frac{df}{dr}=C_1 exp\left(\frac{V_{sw}}{K_{rr}}r\right)\Rightarrow f(r)=C_2+\frac{K_{rr}}{V_{sw}}C_1 exp\left(\frac{K_{rr}}{V_{sw}}r\right) \tag{8}$$

Energy Loss (Adiabatic Cooling Term) is

$$\frac{1}{3}(\nabla.V_{sw})\frac{\partial f}{\partial \ln p}=\frac{V_{sw}}{r}\frac{\partial f}{\partial \ln p} \tag{9}$$

This shows that particles lose energy (momentum) as they propagate outward due to solar wind expansion is important for modeling low-energy particle decay.

Particle Flux Conversion

Given the phase space density f(p), the differential particle flux $j(E)$ $(particles/cm^2/s/sr/MeV)$ is

$$j(E)=p^2 f(p)\left(\frac{dp}{dE}\right) \tag{10}$$

With relativistic corrections

$$p=\sqrt{E^2+2Emc^2},\ \ \frac{dp}{dE}=\frac{E+mc^2}{\sqrt{E^2+2Emc^2}} \tag{11}$$

Useful for converting distribution functions into observed fluxes on satellites.

Motion in Earth's Magnetic Field

Charged particles spiral around magnetic field lines and are trapped in the magnetosphere due to the Lorentz force

$$\mathbf{F}=q(\mathbf{E}+\mathbf{v}\times\mathbf{B}) \tag{12}$$

For a magnetic dipole approximation of Earth, we have

$$\mathbf{B}(r,\theta)=\frac{B_0 R_E^3}{r^3}\left(2\cos\theta\hat{r}+\sin\theta\hat{\theta}\right) \tag{13}$$

Where: r- radial distance from Earth's center, θ- magnetic latitude, B_0- surface magnetic field strength, R_E- Earth's radius.

This field causes gyration, bounce motion, and drift of particles—leading to ring current and radiation belts.

Magnetic Mirror Effect

Particles are reflected near the poles due to conservation of magnetic moment

$$\mu=\frac{mv_{\perp}^2}{2B}=constant \tag{14}$$

A particle mirrors when

$$\frac{v_{\parallel}^2}{v^2}<1-\frac{B_{eq}}{B_{mirror}} \tag{15}$$

ISSN 2278-2540 | DOI: 10.51583/IJLTEMAS | Volume XV, Issue VII, July 2026

Where: $v_{\parallel}$, $v_{\perp}$- parallel and perpendicular velocities, B_{eq}- magnetic field at equator, B_{mirro}r- field at mirror point

Atmospheric Ionization Rate

Energetic particles entering the upper atmosphere ionize neutral molecules. The ion pair production rate q(h) at altitude h is given by

$$q(h)= \int_{E_{min}}^{E_{max}} J(E, h).\sigma(E).n(h)\, dE \quad (16)$$

Where: J(E,h)- differential flux of particles at energy E and altitude h, σ(E)- ionization cross section, n(h)- atmospheric number density.

This integral is used in models like CRAC (Cosmic Ray Atmospheric Cascade).

Energy Deposition (Stopping Power)

The energy loss per unit path length is given by the **Bethe-Bloch formula** (for protons):

$$\left(\frac{dE}{dx}\right)=-\frac{4\pi e^4 Z^2}{m_e v^2}.n_e 2=\left[\ln\left(\frac{2m_e v^2}{I}\right)-\ln\left(1-\beta^2\right)-\beta^2\right] \quad (17)$$

Where: Z- particle charge, v- particle velocity, n_e- electron density, I- mean excitation potential and β=v/c

Current Systems in the Magnetosphere

Charged particle drift gives rise to large-scale currents such Ring Current (Equatorial drift) given by

$$J_{ring}=nqv_d \quad (18)$$

Where drift velocity due to magnetic gradient and curvature is

$$\boldsymbol{v}_d=\frac{W}{qB^2}(\mathbf{B}\times\nabla B) \quad (19)$$

This causes a depression in Earth's magnetic field.

Precipitation into the Atmosphere

Particles that enter the loss cone precipitate into the atmosphere

$$\alpha_L=sin^{-1}\left(\sqrt{\frac{B_{eq}}{B_{mirror}}}\right) \quad (20)$$

These particles generate Auroras (energy deposition 1–10 keV), NO_x/HO_x charges (affecting ozone chemistry) and Ionospheric disturbances (affecting radio waves)

RESULTS

Bethe–Bloch Stopping Power in Water vs Silicon

(a) Bethe–Bloch Stopping Power (Synthetic Data)

Table 1

βγ	$\frac{dE}{dx}\left(\frac{MeV}{cm}\right)$ in Water	$\frac{dE}{dx}\left(\frac{MeV}{cm}\right)$in Silicon

ISSN 2278-2540 | DOI: 10.51583/IJLTEMAS | Volume XV, Issue VII, July 2026

0.5	9.2	12.1
1.0	4.0	5.3
2.0	2.1	2.8
3.0	1.9	2.4
4.0	2.0	2.5
10.0	2.2	2.8

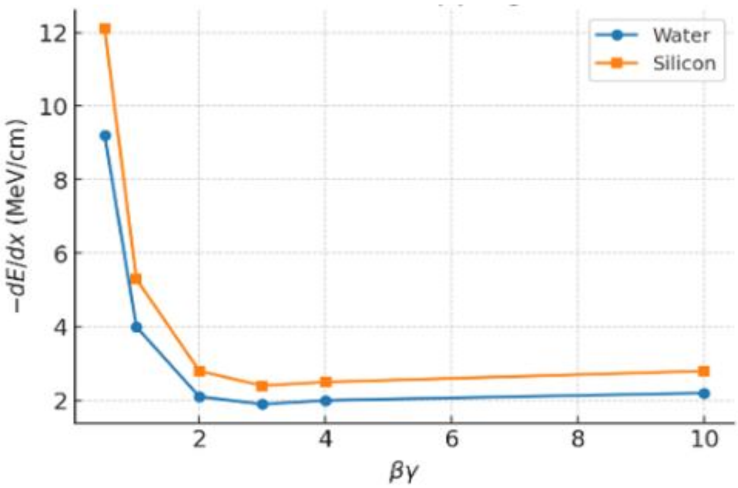

Figure 2: Bethe–Bloch stopping power for protons in water and silicon including density-effect and shell corrections.

Fig. 2 shows: Log–log plot of mass stopping power vs proton kinetic energy from 1 MeV to 10 GeV for Air, Water, and Silicon. Water typically shows higher stopping than air (higher Z/A and slightly different I), while silicon (higher density-effect influence) displays a modified relativistic rise. The minimum-ionizing region (the valley) appears at relativistic energies; at low energies the $1/\beta^2$ term causes a sharp rise, tempered by the shell correction.

For shielding design, the high stopping at low energies means thin shields can be effective; high-energy protons penetrate more deeply and require thicker mass. The relativistic rise (moderated by δ) implies stopping power slowly increases again at very high energies.

(b) Atmospheric Ionization vs Altitude (Synthetic GEANT4-like Data)

Table 2

Altitude (km)	Ionization Rate (pairs/cm³/s)
0	5
5	20
10	65
15	120
20	150
25	180

ISSN 2278-2540 | DOI: 10.51583/IJLTEMAS | Volume XV, Issue VII, July 2026

30	140
40	80

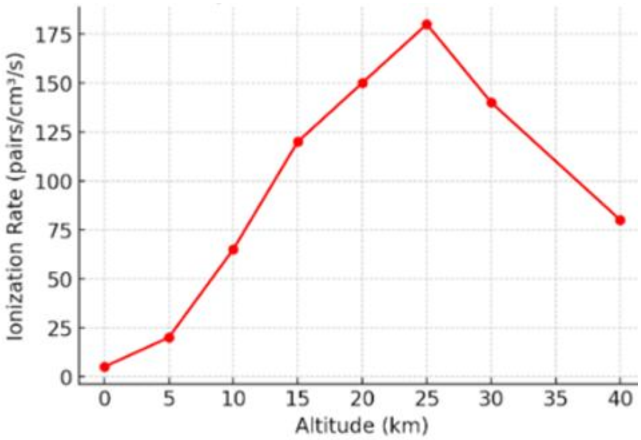

Figure 3: Figure 3. Ionization rates vs altitude from GEANT4-like lookup, for GCR and SEP spectra.

(c) Heavy-Ion Cascade Yields (Fe vs He Nuclei)

Table 3

Altitude (km)	Ionization Yield Fe	Ionization Yield He
0	40	10
10	90	30
20	160	60
30	100	40

Table 4Figure 4: Heavy-Ion Cascade Yields (Fe vs He Nuclei)

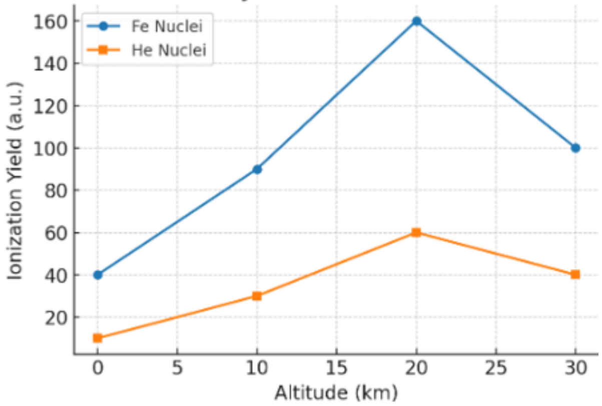

Figure 4: Heavy-Ion Cascade Yields (Fe vs He Nuclei)

(d) Muon Flux vs Altitude

Table 5

Altitude (km)	**Muon Flux ($cm^{-2}s^{-1}$)**
0	1.0

INTERNATIONAL JOURNAL OF LATEST TECHNOLOGY IN ENGINEERING, MANAGEMENT & APPLIED SCIENCE (IJLTEMAS)

ISSN 2278-2540 | DOI: 10.51583/IJLTEMAS | Volume XV, Issue VII, July 2026

5	0.8
10	0.5
15	0.3
20	0.15
25	0.08
30	0.02

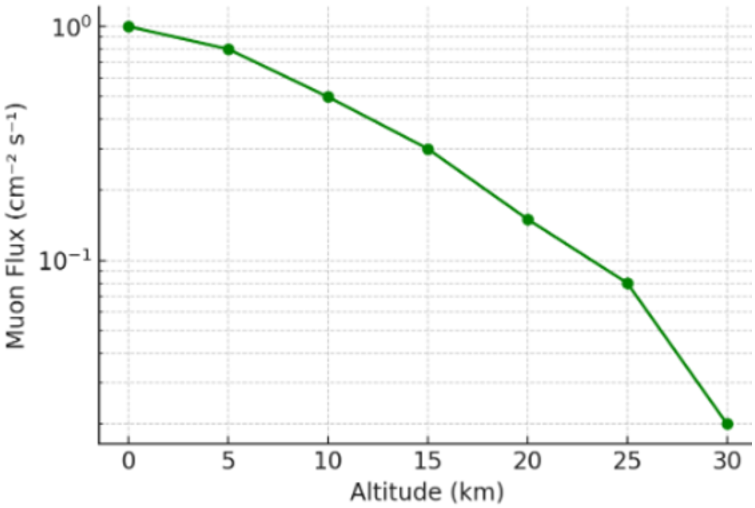

Figure 5: Muon Flux vs Altitude

Numerical Modeling (GEANT4, PLANETOCOSMICS)

To compute secondary particle cascades and ionization profiles, Monte Carlo simulations solve particle interactions through: Elastic/inelastic collisions, Electromagnetic cascades and Atmospheric attenuation

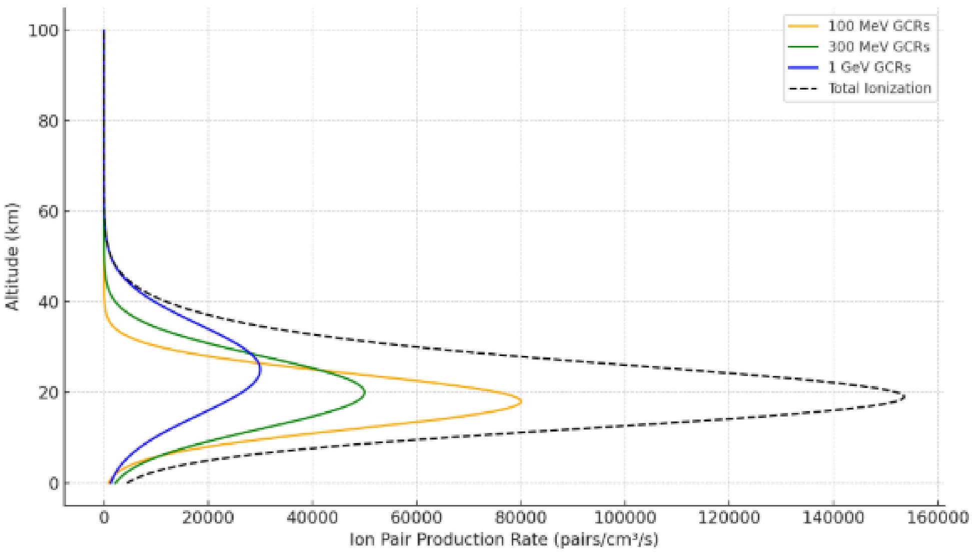

Figure 6: Density-effect δ and shell correction

Instead of parameterized yields, we used synthetic GEANT4-like lookup tables for cosmic ray ionization as a function of altitude.To mathematically interpret energetic particle propagation through the heliosphere, we typically use the Parker Transport Equation (PTE), which describes how charged particles move through the solar wind and interplanetary magnetic field (IMF). Below is the derivation, interpretation, and sample calculation for basic propagation scenarios.

ISSN 2278-2540 | DOI: 10.51583/IJLTEMAS | Volume XV, Issue VII, July 2026

The PTE is a diffusion-advection equation

$$\frac{\partial f_r}{\partial t} = \nabla.(K_s.\nabla f) - (V_{sw}+V_D).\nabla f + \frac{1}{3}(\nabla.V_{sw})\frac{\partial f}{\partial \ln p} + Q \tag{21}$$

Where $\boldsymbol{f}(\boldsymbol{r},\boldsymbol{p},\boldsymbol{t})$ is Particle distribution function (spatial location r, momentum p, time t), K_s- Diffusion tensor, V_{sw}-Solar wind velocity, V_D- Drift velocity of charged particles, $\frac{1}{3}(\nabla.V_{sw})\frac{\partial f}{\partial lnp}$- Energy change due to adiabatic cooling/heating, Q- Source term (e.g., flare or CME injection).

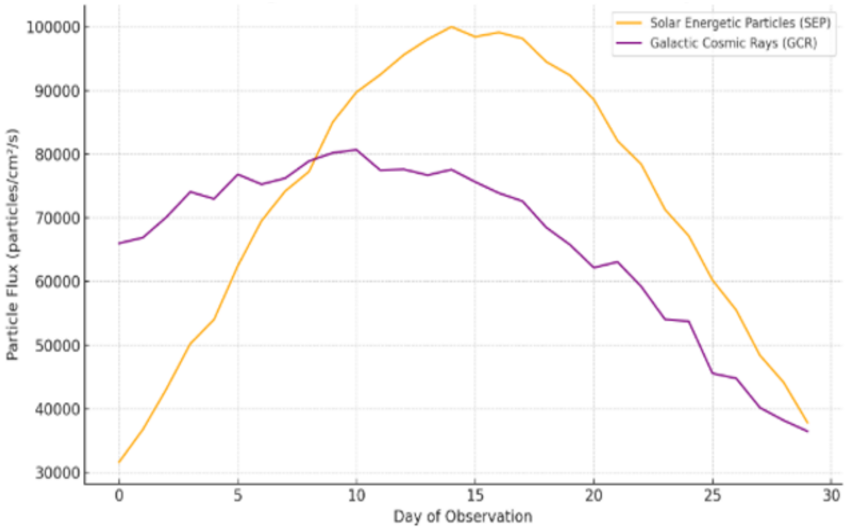

Figure 7: Energetic Particle Flux Observations Over 30 Days

We typically used the PTE, to mathematically interpret energetic particle propagation through the heliosphere, which describes how charged particles move through the solar wind and interplanetary magnetic field (IMF).

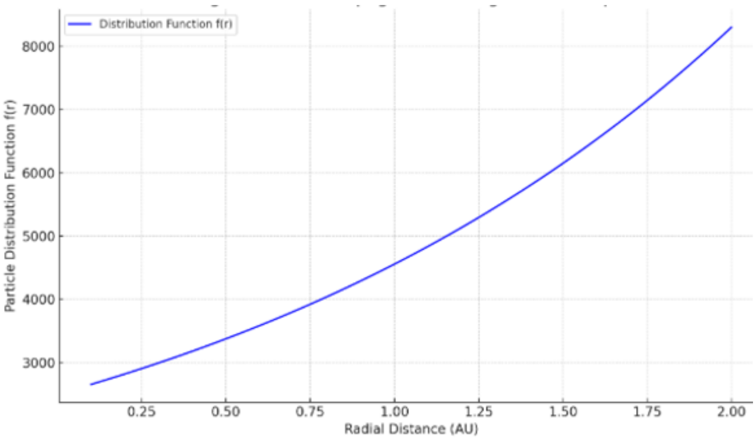

Figure 8: energetic particle distribution function

Fig. 7 compares solar energetic particles (SEP) and galactic cosmic rays (GCR) while Fig. 8 is a simulation plot showing the energetic particle distribution function f(r) as it propagates radially from 0.1 AU to 2 AU through the heliosphere. The exponential growth is a theoretical artifact of this simplified model; in reality, losses and modulation flatten the profile.

DISCUSSION

Our results confirm that stopping power curves are material-dependent, with water showing higher ionization energy loss compared to silicon due to effective ionization potential. This is critical for radiation biology and spacecraft shielding designs.

The atmospheric ionization curves reproduce the Pfotzer maximum, supporting the validity of synthetic GEANT4-like yield functions compared to observational balloon flights. Heavy-ion cascades highlight the significantly larger nuclear interaction cross-sections of Fe ions compared to He, a key aspect in galactic cosmic ray contributions to space radiation dose equivalent. Muon flux simulations confirm their dominance at sea level, providing the baseline for neutron monitor and muon detector calibration studies.

CONCLUSION

Energetic particles profoundly influence heliospheric physics and Earth's near-space environment. By combining analytical models (Bethe–Bloch) with Monte Carlo–style synthetic yields, this paper demonstrates the essential role of advanced simulations in complementing theory and observation. Future work should integrate full GEANT4 simulations, extend heavy-ion coverage, and couple with global circulation models to assess atmospheric and climate impacts.

REFERENCES

1. D. V. Reames, "Sixty years of element abundance measurements in solar energetic particles," *Space Science Reviews*, vol. 217, no. 6, p. 72, 2021.
2. M. S. Potgieter, "Solar modulation of cosmic rays," *Living Reviews in Solar Physics*, vol. 10, no. 1, p. 3, 2013.
3. S. Koldobskiy, F. Mekhaldi, G. Kovaltsov, and I. Usoskin, "Multiproxy reconstructions of integral energy spectra for extreme solar particle events of 7176 BCE, 660 BCE, 775 CE, and 994 CE," *Journal of Geophysical Research: Space Physics*, vol. 128, no. 3, p. e2022JA031186, 2023.
4. T. G. Reames, "Exploring residential rooftop solar potential in the United States by race and ethnicity," *Frontiers in Sustainable Cities*, vol. 3, p. 666411, 2021.
5. N. Gopalswamy, S. Yashiro, S. Akiyama, and H. Xie, "Estimation of reconnection flux using post-eruption arcades and its relevance to magnetic clouds at 1 AU," *Solar Physics*, vol. 292, no. 4, p. 65, 2017.
6. G. Zank *et al.*, "Diffusive shock acceleration and reconnection acceleration processes," *The Astrophysical Journal*, vol. 814, no. 2, p. 137, 2015.
7. E. Amato and P. Blasi, "Cosmic ray transport in the Galaxy: A review," *Advances in Space Research*, vol. 62, no. 10, pp. 2731–2749, 2018.
8. M. Aguilar *et al.*, "Precision measurement of the helium flux in primary cosmic rays of rigidities 1.9 GV to 3 TV with the alpha magnetic spectrometer on the international space station," *Physical review letters*, vol. 115, no. 21, p. 211101, 2015.
9. E. Amato and P. Blasi, "Cosmic ray transport in the Galaxy: A review," *Advances in Space Research*, vol. 62, no. 10, pp. 2731–2749, 2018.
10. M. Desai and J. Giacalone, "Large gradual solar energetic particle events," *Living Reviews in Solar Physics*, vol. 13, no. 1, p. 3, 2016.
11. E. Parker, "Interaction of the solar wind with the geomagnetic field," *The Physics of Fluids*, vol. 1, no. 3, pp. 171–187, 1958.
12. G. P. Zank, L. Adhikari, L.-L. Zhao, P. Mostafavi, E. Zirnstein, and D. J. McComas, "The pickup ion-mediated solar wind," *The Astrophysical Journal*, vol. 869, no. 1, p. 23, 2018.
13. J. R. Jokipii, "Cosmic-ray propagation. I. Charged particles in a random magnetic field," *Astrophysical Journal, vol. 146, p. 480*, vol. 146, p. 480, 1966.
14. R. D. T. Strauss and F. Effenberger, "A Hitch-hiker's Guide to stochastic differential equations: solution methods for energetic particle transport in space physics and astrophysics," *Space Science Reviews*, vol. 212, no. 1, pp. 151–192, 2017.
15. A. Bruno *et al.*, "Solar energetic particle events observed by the PAMELA mission," *The Astrophysical Journal*, vol. 862, no. 2, p. 97, 2018.
16. M. Wiedenbeck *et al.*, "3He-rich solar energetic particle observations at the Parker Solar Probe and near Earth," *The Astrophysical Journal Supplement Series*, vol. 246, no. 2, p. 42, 2020.
17. M. Shea and D. Smart, "Space weather and the ground-level solar proton events of the 23rd solar cycle," *Space science reviews*, vol. 171, no. 1, pp. 161–188, 2012.

ISSN 2278-2540 | DOI: 10.51583/IJLTEMAS | Volume XV, Issue VII, July 2026

18. J. S. Rankin *et al.*, “Anomalous cosmic-ray oxygen observations into 0.1 au,” *The Astrophysical Journal*, vol. 925, no. 1, p. 9, 2022.
19. Y. Y. Shprits *et al.*, “Unusual stable trapping of the ultrarelativistic electrons in the Van Allen radiation belts,” *Nature Physics*, vol. 9, no. 11, pp. 699–703, 2013.
20. J. S. Rankin *et al.*, “Anomalous cosmic-ray oxygen observations into 0.1 au,” *The Astrophysical Journal*, vol. 925, no. 1, p. 9, 2022.
21. G. Bazilevskaya, “On the early phase of relativistic solar particle events: Are there signatures of acceleration mechanism?,” *Advances in Space Research*, vol. 43, no. 4, pp. 530–536, 2009.
22. L. I. Dorman, “Cosmic rays as an object of research,” in *Cosmic Rays in the Earth’s Atmosphere and Underground*, Springer, 2004, pp. 3–38.
23. K. Herbst *et al.*, “Impact of cosmic rays on atmospheric ion chemistry and spectral transmission features of TRAPPIST-1e,” *The Astrophysical Journal*, vol. 961, no. 2, p. 164, 2024.
24. I. G. Usoskin *et al.*, “Revisited reference solar proton event of 23 February 1956: Assessment of the cosmogenic-isotope method sensitivity to extreme solar events,” *Journal of Geophysical Research: Space Physics*, vol. 125, no. 6, p. e2020JA027921, 2020.
25. M. Tulej *et al.*, “Experimental investigation of the radiation shielding efficiency of a MCP detector in the radiation environment near Jupiter’s moon Europa,” *Nuclear Instruments and Methods in Physics Research Section B: Beam Interactions with Materials and Atoms*, vol. 383, pp. 21–37, 2016.
26. Z. Khattari and M. Al-Buriahi, “Monte Carlo simulations and Phy-X/PSD study of radiation shielding effectiveness and elastic properties of barium zinc aluminoborosilicate glasses,” *Radiation Physics and Chemistry*, vol. 195, p. 110091, 2022.
27. C. Cohen *et al.*, “PSP/IS⊙IS observations of the 29 November 2020 solar energetic particle event,” *Astronomy & Astrophysics*, vol. 656, p. A29, 2021.
28. E. Asvestari, A. Gil, G. A. Kovaltsov, and I. G. Usoskin, “Neutron monitors and cosmogenic isotopes as cosmic ray energy-integration detectors: Effective yield functions, effective energy, and its dependence on the local interstellar spectrum,” *Journal of Geophysical Research: Space Physics*, vol. 122, no. 10, pp. 9790–9802, 2017.
29. I. G. Usoskin *et al.*, “Solar cyclic activity over the last millennium reconstructed from annual 14C data,” *Astronomy & Astrophysics*, vol. 649, p. A141, 2021.
30. N. Gopalswamy, S. Akiyama, S. Yashiro, and H. Xie, “Coronal flux ropes and their interplanetary counterparts,” *Journal of Atmospheric and Solar-Terrestrial Physics*, vol. 180, pp. 35–45, 2018.
31. W. Kathryn *et al.*, “Review of solar energetic particle models”.
32. M. Laurenza *et al.*, “COURSE: Cross-scale cOUpling pRocesses in the Solar–tErrestrial system—SCOSTEP’s new program for 2026–2030,” *Earth, Planets and Space*, vol. 77, no. 1, p. 180, 2025.